

# Study of the Electric Field Around a Metal Oxide Surge Arrester: Measurement and Simulation

Christodoulou C A, Spanias C A, Kontargyri V T, Gonos I F, Stathopoulos I A  
(High Voltage Laboratory, School of Electrical and Computer Engineering, National Technical University  
of Athens Iroon Polytechniou 9, 15780, Zografou Campus, Athens, Greece)

**Abstract:** The study of the electric field around a surge arrester is useful for design procedures and diagnostic tests. The current work computes the electric field around a medium voltage gapless surge arrester using 2D and 3D representation of the arrester. The 2D simulation design, which is described in IEC 60099-4 Standard, cannot include the non symmetrical parts of the arrester geometry and the test arrangement. 3D simulation procedures have the advantage that takes into account these asymmetries, giving more accurate results for each measurement position. In order to confirm the suitability of the created models, the simulation results of the electric field, using the 2D and 3D edition of PC Opera, are compared with recorded measurements, which are obtained in laboratory using appropriate calibrated field meters.

**Key words:** surge arresters; electric field; 2D and 3D simulation; voltage distribution; uncertainties' computation

**DOI:** 10.3969/j. issn. 1003-6520. 2013. 08. 000

**Article No:** 1003-6520(2013)08-0000-00

## 0 Introduction

Surge arresters are semiconductor devices, which are used in electrical power systems in order to protect them against lightning and switching overvoltages. Arresters are installed between phase and earth and act as bypath for the overvoltage impulse, since they are designed to be insulators for nominal operating voltage, conducting at most few milliamperes of current and good conductors, when the voltage of the line exceeds design specifications to pass the energy of the overvoltage wave to the ground. Even though a great number of arresters, which are gapped arresters with resistors, made of SiC are still in use, the arresters installed today are almost all metal oxide arresters without gaps, which means arresters with resistors made of metal oxide<sup>[1-2]</sup>. The distinctive feature of a metal oxide arrester is its extremely nonlinear voltage-current characteristic, rendering unnecessary the disconnection of the resistors from the line through serial spark gaps, as it is found in the arresters with SiC resistors. Additionally, metal oxide arresters are inherently faster-acting than the gapped type, since there is no time delay due to series air gaps extinguishing the current<sup>[3]</sup>.

The basic parts of a metal oxide surge arresters are the cylindrical metal-oxide resistor blocks (varistor), the insulating housing, and the electrodes.

Between the varistor column and the polymeric housing there is a glassfibre structure, that either completely encloses the resistor blocks or exerts sufficient force on the ends of the stack to hold the metal oxide blocks firmly together.

The electric field around a surge arrester is influenced by

the geometry of the arrester and the electrical characteristics of the participating materials<sup>[4]</sup>. Electric field modeling helps the designers know and consider the important factors affecting the maximum field intensity in the arrester, avoiding too high potential gradients inside and outside the arrester, especially during the transient conditions, a phenomenon which can cause damages to the arrester insulating system that brings it to a premature failure<sup>[5]</sup>. Hence, the knowledge of the electric field can be useful for on line and laboratory diagnostic tests<sup>[6-7]</sup>, in order to check the condition of the varistor or the existence of moisture or pollution on the insulation surface<sup>[1-4]</sup>.

The IEC 60099-4 Standard gives analytical instructions for the surge arresters modeling in two dimensions<sup>[8]</sup>; the 2D simulation cannot represent the non-symmetrical parts of the arresters and the system configuration (such as the arresters electrodes, the high voltage conductors, the grounding system etc) that may affect the electric field and potential distribution. Additionally, many researches have computed the electric field around a metal oxide arrester using appropriate simulation toolboxes (PC Opera, Comsol, etc), examining different cases, such as surface pollution, broken sheds, etc<sup>[4-5,9-12]</sup>.

Aim of this paper is the experimental and theoretical study of the electric field distribution around a medium voltage metal oxide gapless polymeric (silicon rubber) surge arrester<sup>[13]</sup>. For this reason, the current work uses additionally 3D simulation analysis, designing in three dimensions for the examined arrester. In order to show the differences between 2D and 3D analysis the simulation results are compared to experimental measurements, obtained in the High Voltage

Laboratory of the National Technical University of Athens (NTUA).

**1 Measurements Arrangement**

Fig.1 presents the test configuration for the measurement of the electric field around the arrester. The measurements were carried out in the High Voltage Laboratory of the NTUA, for a typical medium voltage metal oxide gapless polymeric housing surge arrester that Hellenic Power Corporation S.A. uses for the protection of the distribution network installations, applying 12 kV that corresponds to the nominal value of a typical medium voltage power system of the Hellenic network. The non-linear resistance of the examined gapless surge arrester is consisted of ZnO varistor discs connected in series and surrounded from fiber glass. The polymeric external insulation has six sheds, so the whole geometry of the arrester is symmetrical, excepting the electrodes. The high voltage and the earth electrode are non symmetrical (as it is shown in Fig.2), influencing the measurement results of the electric field.

The applied voltage was measured in the low voltage side of the transformer with a calibrated digital voltmeter<sup>[14]</sup>, taking into account the transformer’s ratio. In Fig.1,  $U_1$  is the voltage of the transformer’s primary,  $U_2$  is the voltage of the transformer’s secondary. The electric field around the surge arrester was measured using two appropriate calibrated field meters (Narda and PMM 8053)<sup>[15-16]</sup>. Each one of both alternatively used sensors (EFA 300 and EHP-50B correspondingly) was moved in different directions: on the horizontal plane, in various distances ( $d$ ) along five different axes (as it is shown in Fig.3), considering the shape and the symmetry of the arrester, and in various heights ( $h$ ).

**2 Uncertainties’ Computation**

The measurements of the electric field were carried out using two different appropriately calibrated instruments and sensors, in order to confirm the correctness of the experimental records and to show that the quality of the measurement results is strongly related to the used instrument. Each measurement is accompanied with its total uncertainty and for each point repetitive measurements were taken in order to evaluate the type A uncertainty. The user of the field meters stays at least 10 m away from the sensor, thus avoiding interferences to the electric field and measurement.

Analytically, uncertainty is a parameter characterizing the dispersion of the values attributed to a measured quantity. The uncertainty has a probabilistic basis and reflects incomplete

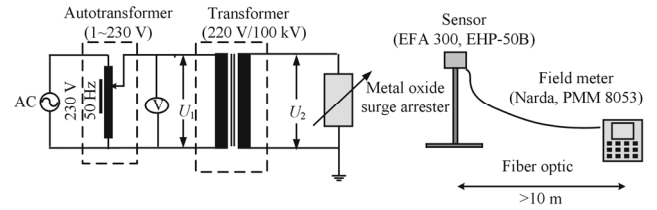


**Fig.1 Experimental set-up used for the measurement of the electric field distribution**



**Fig.2 Examined polymeric housing gapless metal oxide surge arrester**

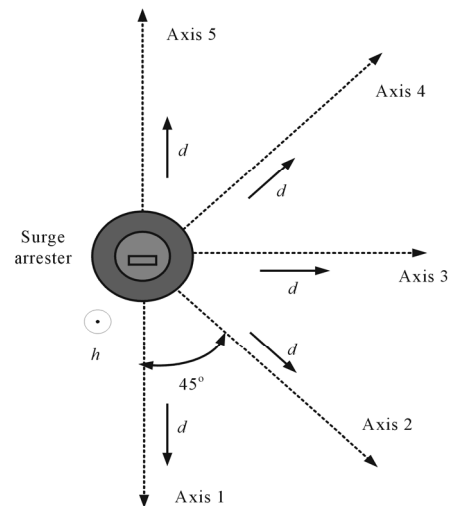


**Fig.3 Topology of the measurement axes**

knowledge of the quantity. All measurements are subject to uncertainty and a measured value is only complete if it is accompanied by a statement of the associated uncertainty. When a quantity is measured, the outcome depends on the measuring system, the measurement procedure, the skill of the operator, the environment, and other effects. Even if the quan-

tity were to be measured several times, in the same way and in the same circumstances, a different measured value would in general be obtained each time, assuming that the measuring system has sufficient resolution to distinguish the values. Uncertainties are categorized in type A (or random uncertainty) and type B (or systematic uncertainty)<sup>[17]</sup>. Type A uncertainty  $u_r$  is computed with statistical analysis of series measurements, using equation (1):

$$u_r = \frac{ts_r}{\sqrt{n}} \quad (1)$$

where  $t$  is the student's factor depending on the number of the measurements ( $n$ ) for a given confidence level and  $s_r$  the standard deviation.

Type B uncertainty  $u_s$  is not evaluated statistically, but is estimated based on the uncertainty of the measuring system (stated in the calibration certificate), the drift in the value of the scale factor of the measuring system, the resolution of each instrument and the fact that the conditions during the use of a measuring system are different from those on the calibration (e.g. different temperature).

The derivation of the overall expanded uncertainty  $u$  is based on the square root of the sum of the squares of the systematic and random uncertainty contributions:

$$u = k\sqrt{u_r^2 + u_s^2} \quad (2)$$

where  $k$  is the coverage factor depending on the desired confidence level.

The type B uncertainty of the field meters is evaluated, using the calibration certificates, according to equation (3):

$$u_s = \sqrt{\Delta E_R^2 + \Delta E_C^2 + \Delta E_F^2} \quad (3)$$

where  $\Delta E_R$  is the contribution (rectangular) of the uncertainty of the reading,  $\Delta E_C$  is the contribution (normal) of the uncertainty of the calibration,  $\Delta E_F$  is the contribution (rectangular) of the uncertainty of the non homogeneity of the field.

The type B uncertainty of the Narda/EFA 300 field meter is calculated to be 2.32% and that of the PMM 8053 to be 4.1%, for 50 Hz and electric field range from 10 V/m to 500 V/m and 4.4% from 500 V/m to 100 kV/m.

### 3 Measurement Results

Table 1~Table 5 present the measurements of the electric field for each position and for each axis (1 to 5 according to Fig.3) for both instruments (Narda/EFA 300 and PMM 8053), when the voltage applied on the arrester is equal to 12 kV, which corresponds to the nominal value of a typical medium voltage power system of the Hellenic network.  $E_{1,Narda}$  corresponds to the measured electric field for the axis 1 using the Narda EFA 300 field meter,  $u_{1,Narda}$  corresponds to the total uncertainty for the axis 1 using the Narda EFA 300 field meter,  $E_{1,PMM}$  corresponds to the measured electric field for the axis 1 using the PMM 8053 field meter,  $u_{1,PMM}$  corresponds to the total uncertainty for the axis 1 using the PMM 8053 field meter,  $E_{2,Narda}$  corresponds to the measured electric field for the axis 2 using the Narda EFA 300 field meter,  $u_{2,Narda}$  corresponds to the total uncertainty for the axis 2 using the Narda EFA 300 field meter,  $E_{2,PMM}$  corresponds to the measured electric field for the axis 2 using the PMM 8053 field meter,  $u_{2,PMM}$  corresponds to the total uncertainty for the axis 2 using the PMM 8053 field meter, etc. Table 1~Table 5 include, also, the total uncertainty for each measurement according to eq.(2).

Table 1 Electric field for each distance and height along axis 5

d/m	h=13 cm				h=21 cm				h=29 cm			
	$E_{1,Narda}/(V \cdot m^{-1})$	$u_{1,Narda}/\%$	$E_{1,PMM}/(V \cdot m^{-1})$	$u_{1,PMM}/\%$	$E_{1,Narda}/(V \cdot m^{-1})$	$u_{1,Narda}/\%$	$E_{1,PMM}/(V \cdot m^{-1})$	$u_{1,PMM}/\%$	$E_{1,Narda}/(V \cdot m^{-1})$	$u_{1,Narda}/\%$	$E_{1,PMM}/(V \cdot m^{-1})$	$u_{1,PMM}/\%$
0.5	3 803	5.11	4 256	9.24	3 987	5.11	4 696	9.64	4 050	4.95	4 759	9.17
0.8	1 663	5.02	1 947	9.42	1 681	4.81	2 031	9.54	1 740	5.09	2 080	9.23
1.1	909.5	4.77	981.5	9.16	924.2	4.97	1 017	9.08	960.3	4.75	1 082	9.55
1.4	537.7	4.82	562.8	9.06	554.3	5.02	591.3	9.21	566.1	4.79	619.5	9.44
1.7	331	5.01	349.7	9.42	340.3	4.82	355.9	9.24	342.4	4.95	383.8	9.20
2	214.5	4.90	220.5	9.31	221.5	4.93	235.3	9.47	224.4	5.01	253.2	9.31

Table 2 Electric field for each distance and height along axis 2

d/m	h=13 cm				h=21 cm				h=29 cm			
	$E_{2,Narda}/(V \cdot m^{-1})$	$u_{2,Narda}/\%$	$E_{2,PMM}/(V \cdot m^{-1})$	$u_{2,PMM}/\%$	$E_{2,Narda}/(V \cdot m^{-1})$	$u_{2,Narda}/\%$	$E_{2,PMM}/(V \cdot m^{-1})$	$u_{2,PMM}/\%$	$E_{2,Narda}/(V \cdot m^{-1})$	$u_{2,Narda}/\%$	$E_{2,PMM}/(V \cdot m^{-1})$	$u_{2,PMM}/\%$
0.5	3 739	5.04	4 276	9.89	3 991	5.03	4 468	9.51	4 129	4.90	4 659	9.44
0.8	1 646	4.86	1 833	9.66	1 702	4.92	1 912	9.44	1 771	5.14	2 067	9.69
1.1	844.3	4.97	935.7	9.35	905.2	5.15	995.8	9.24	911	4.94	1 086	9.35
1.4	493.6	5.04	534.2	9.44	534.7	4.91	572.6	9.23	540.5	5.06	632.4	9.40
1.7	304.9	5.15	328.8	9.48	330.9	4.91	347.5	9.07	336.2	5.02	390.4	9.53
2	200.9	5.28	216.2	9.55	216.2	4.80	229.7	9.10	221.5	5.03	250.9	9.42

**Table 3 Electric field for each distance and height along axis 3**

<i>d/m</i>	<i>h</i> =13 cm				<i>h</i> =21 cm				<i>h</i> =29 cm			
	$E_{3,Narda}/(V \cdot m^{-1})$	$u_{3,Narda}/\%$	$E_{3,PMM}/(V \cdot m^{-1})$	$u_{3,PMM}/\%$	$E_{3,Narda}/(V \cdot m^{-1})$	$u_{3,Narda}/\%$	$E_{3,PMM}/(V \cdot m^{-1})$	$u_{3,PMM}/\%$	$E_{3,Narda}/(V \cdot m^{-1})$	$u_{3,Narda}/\%$	$E_{3,PMM}/(V \cdot m^{-1})$	$u_{3,PMM}/\%$
0.5	3 726	5.02	4 139	9.46	3 835	5.08	4 421	9.38	3 981	4.84	4 586	9.57
0.8	1 625	5.07	1 839	9.88	1 651	4.81	1 879	9.50	1 653	4.76	2 046	9.19
1.1	825.5	5.28	936.9	9.55	859.1	5.24	986.2	9.15	869.9	4.91	1 054	9.66
1.4	489.1	4.85	544.5	9.65	510.4	5.17	569.2	9.69	523.1	5.08	632.1	9.55
1.7	300.9	4.82	332.6	9.78	316.9	4.97	352.8	9.31	323.5	5.02	393.2	9.33
2	195.2	5.12	217.6	9.45	206.5	4.92	229.6	9.53	213.5	4.69	257.4	9.24

**Table 4 Electric field for each distance and height along axis 4**

<i>d/m</i>	<i>h</i> =13 cm				<i>h</i> =21 cm				<i>h</i> =29 cm			
	$E_{4,Narda}/(V \cdot m^{-1})$	$u_{4,Narda}/\%$	$E_{4,PMM}/(V \cdot m^{-1})$	$u_{4,PMM}/\%$	$E_{4,Narda}/(V \cdot m^{-1})$	$u_{4,Narda}/\%$	$E_{4,PMM}/(V \cdot m^{-1})$	$u_{4,PMM}/\%$	$E_{4,Narda}/(V \cdot m^{-1})$	$u_{4,Narda}/\%$	$E_{4,PMM}/(V \cdot m^{-1})$	$u_{4,PMM}/\%$
0.5	3 432	5.24	3 483	9.82	3 663	5.06	3 545	9.86	3 798	5.19	3 845	9.67
0.8	1 548.1	5.35	1 563	9.66	1 595	5.27	1 610	9.49	1 601	4.98	1 653	9.93
1.1	795.1	5.12	832.7	9.22	826.9	5.33	855.1	9.21	839.7	5.03	859.9	9.47
1.4	465.9	4.95	470.6	9.91	483.2	5.01	506.4	9.77	501.1	4.95	547.5	9.64
1.7	284.5	4.79	298.7	9.42	301.3	4.72	308.8	9.40	310	5.09	338.7	9.35
2	184.7	4.85	188.9	9.24	192.5	4.98	205.9	9.19	203	4.69	208.1	9.26

**Table 5 Electric field for each distance and height along axis 5**

<i>d/m</i>	<i>h</i> =13 cm				<i>h</i> =21 cm				<i>h</i> =29 cm			
	$E_{5,Narda}/(V \cdot m^{-1})$	$u_{5,Narda}/\%$	$E_{5,PMM}/(V \cdot m^{-1})$	$u_{5,PMM}/\%$	$E_{5,Narda}/(V \cdot m^{-1})$	$u_{5,Narda}/\%$	$E_{5,PMM}/(V \cdot m^{-1})$	$u_{5,PMM}/\%$	$E_{5,Narda}/(V \cdot m^{-1})$	$u_{5,Narda}/\%$	$E_{5,PMM}/(V \cdot m^{-1})$	$u_{5,PMM}/\%$
0.5	3 551	5.09	3 637	9.77	3 619	5.03	3 689	9.74	3 681	5.38	3 762	9.83
0.8	1 584.1	5.14	1 593	9.62	1 585	5.31	1 606	9.89	1 649	4.91	1 681	9.71
1.1	807.4	5.50	818.7	9.23	840.1	5.14	850.3	9.18	851.9	5.25	891	9.21
1.4	478.8	4.91	490.7	9.82	494.5	5.22	501.7	9.78	495.8	5.14	503.2	9.78
1.7	293.4	5.12	306.3	9.41	303.2	4.90	310.8	9.39	304.3	5.03	317.4	9.40
2	190	4.78	191.5	9.23	201	4.84	212.7	9.42	202.6	5.28	218.1	9.24

Due to the fact that the arrester is not symmetrical, the measurement results are little different for the same height (*h*) and distance (*d*), dependent on the examined axis. The measurements were carried out for both broadband (5 Hz~2 kHz) and badpass (50 Hz) cases, but there were not significant differences, since there were no other electric fields in the laboratory and the input voltage did not have harmonics. So, in the current work only the Bandpass filter measurements are presented.

#### 4 Two and Three Dimensional Simulations

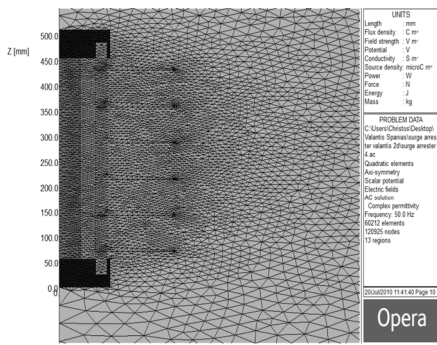
The electric field for given heights and distances is different for each axis, since it is influenced by the non-symmetrical geometry of the arrester. 2D simulation, ignoring these asymmetries, cannot represent these changes for each axis, so there is need for 3D design of the sample. For this reason, the sample is designed and analyzed using 2D and 3D edition of the PC Opera, a Finite Element Analysis program for two and three dimensional electromagnetic design<sup>[18-19]</sup>, and the theoretical results are compared to the recorded measurements.

Fig.4 (a) presents the designed surge arrester model in the 2D edition of PC Opera, ignoring the non symmetrical parts of the sample and the test arrangement geometry. The dielectric

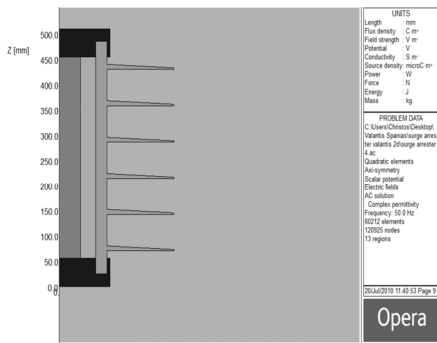
permittivity is 100 for the varistor, 4.6 for the fiber glass, 3.9 for the external insulation and 1 for the air around the arrester. The conductivity of the high voltage and earth electrodes is  $10^6$  S/m. In order to increase the accuracy of the results, the density of the finite element mesh was increased in the critical regions inside and around the arrester (as it is shown in Fig.4 (b)), creating 60212 elements and 120925 nodes.

Fig.5 shows the electric field and the potential inside and around the surge arrester, as they were computed using 2D PC Opera.

The 2D computation does not include the asymmetries of the high voltage and earth electrodes and of the total test arrangement configuration (voltage and earth conductors), which influences the electric field and potential distribution. In order to obtain more accurate results, the examined arrester was designed using the 3D edition of PC Opera. Fig.6 presents the developed 3D model; the electric characteristics of the arrester's materials are the same as in the 2D computations. The mesh was, also, more dense in the critical regions inside and around the arrester, creating 1323551 elements and 226167 nodes. Fig.7 shows the electric field and the potential inside and around the surge arrester, as they were computed using 3D PC Opera.

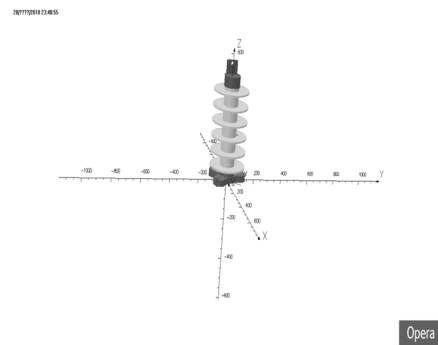


(a) 2 D arrester's model

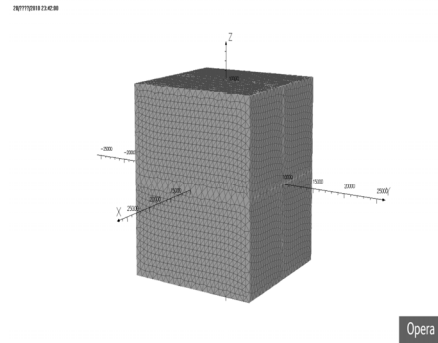


(b) Created mesh

Fig.4 2D arrester's model and the created mesh

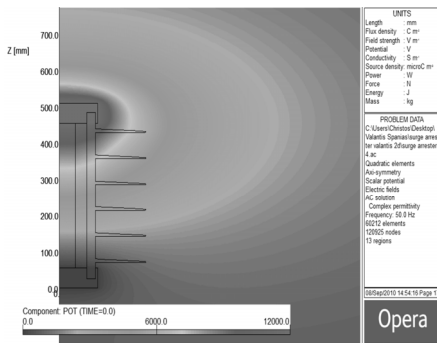


(a) 3D arrester's model

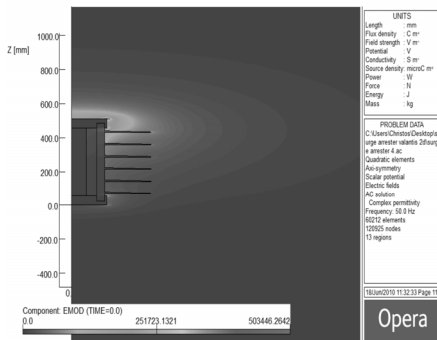


(b) Created mesh

Fig.6 3D arrester's model and the created mesh

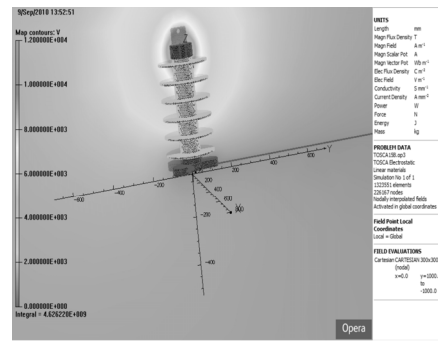


(a) Potential distribution

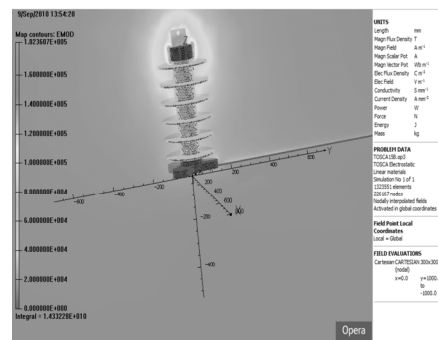


(b) Electric field distribution

Fig.5 Potential and electric field distribution using 2D PC Opera



(a) Potential distribution



(b) Electric field distribution

Fig.7 Potential and electric field distribution using 3D PC Opera

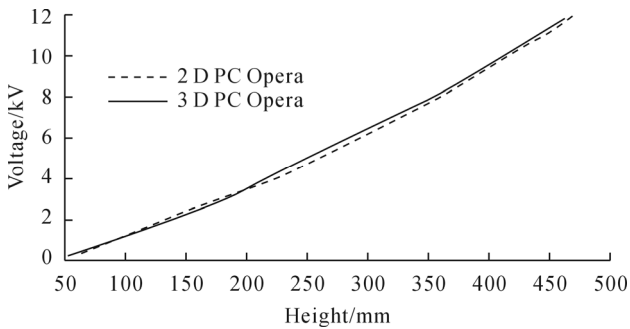
Fig.8 presents the voltage distribution along the varistor of the arrester, obtained from the 2D and 3D edition of PC Opera correspondingly. The voltage distribution is not uniform, due

to the stray capacitances, with the maximum voltage stress appearing in the upper part of the arrester.

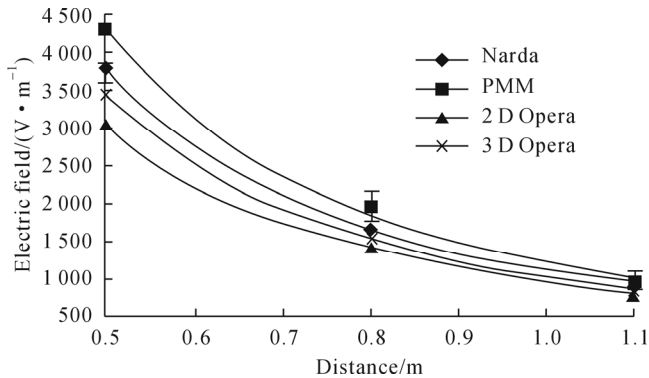
**5 Comparison of Experimental and Simulation Results**

Fig.9~Fig.18 present in common diagrams the electric field for each axis, obtained from the PC Opera and the laboratory measurements, versus distance. A good agreement has been achieved comparing the experimental and the simulation results, especially for the 3D model. The 3D computations present lower error from the measured values, since the 3D model is more precise, due to the fact that takes into account the non symmetrical parts of the arrester and the experiment configuration. The 3D results, considering details of the designed parts of the arrester, are very close to the real recorded measurements. So, 3D analysis is proved to be more appropriate in cases of intense assymetries of the examined device, giving more accurate predictions of the electric field for any position around the arrester.

3D analysis gives more accurate results, since it includes the non-symmetrical parts of the arrester, computing the electric field for the same axes that the measurements were carried out. 3D simulation gives the ability to obtain results for different axes, approaching the actual electric field distribution of the arrester. In contrast to 2D simulation, 3D simulation uses the axi-symmetry of the arrester and produces a unique value of the field for each length and height.



**Fig.8 Comparison of the voltage distribution along varistor using 2D and 3D PC Opera**



**Fig.9 Electric field for axis 1 and height 13 cm**

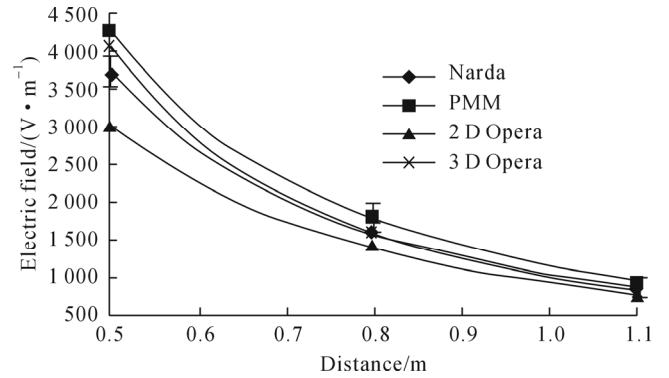


**Fig.10 Electric field for axis 2 and height 13 cm**

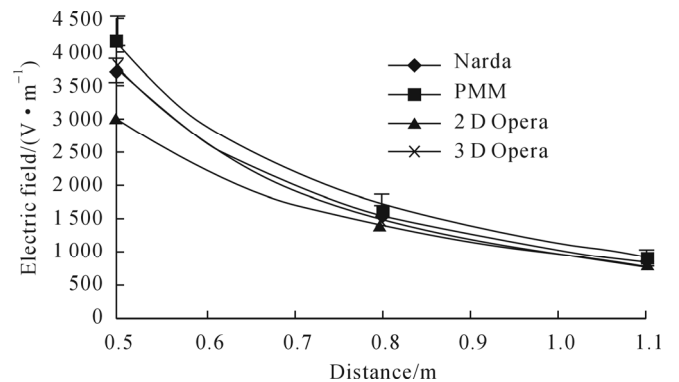


**Fig.11 Electric field for axis 3 and height 13 cm**

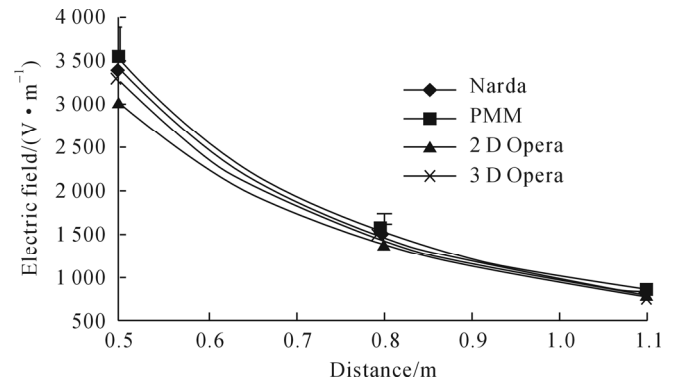


**Fig.12 Electric field for axis 4 and height 13 cm**

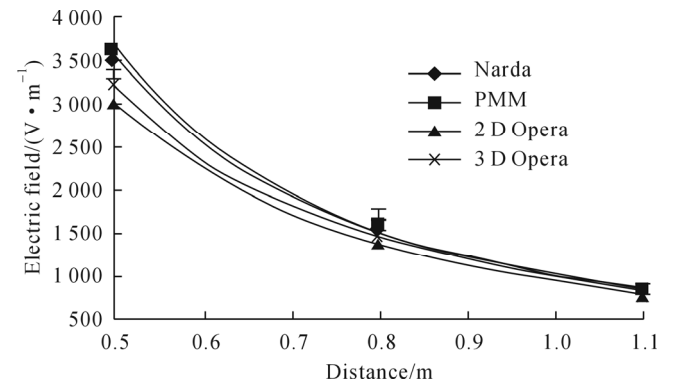


**Fig.13 Electric field for axis 5 and height 13 cm**

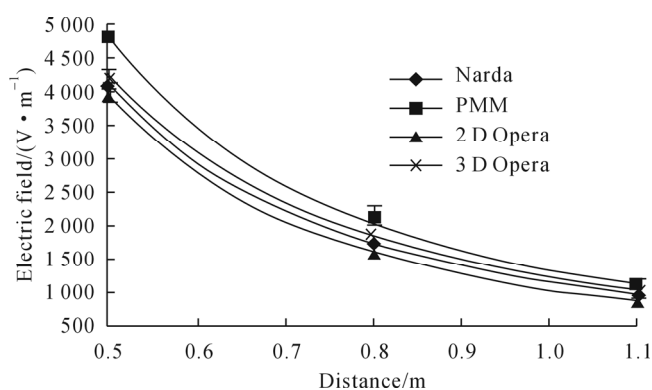


Fig.14 Electric field for axis 1 and height 29 cm

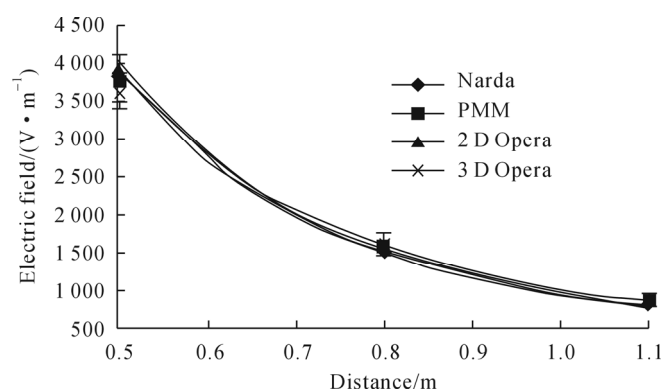


Fig.18 Electric field for axis 5 and height 29 cm

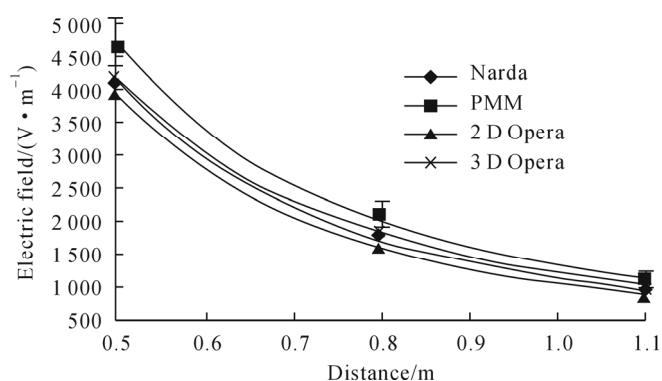


Fig.15 Electric field for axis 2 and height 29 cm

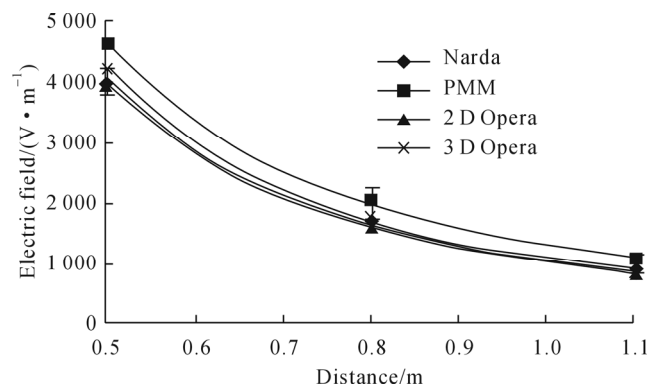


Fig.16 Electric field for axis 3 and height 29 cm

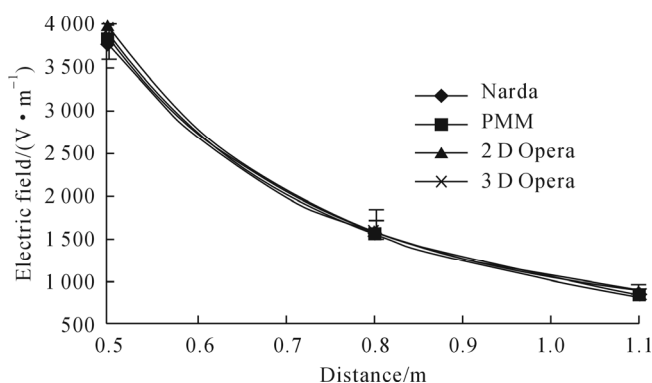


Fig.17 Electric field for axis 4 and height 29 cm

## 6 Conclusions

In the current work, the electric field around a metal oxide surge arrester is measured and the experimental results are compared to results obtained using the 2D and 3D edition of PC Opera. A very good agreement has been ascertained, especially for the 3D simulation values, since the 3D models takes into account the non symmetric parts of the arrester and the overall experiment configuration. The results show that in case of significant assymetries of the arresters geometry, there is need of 3D computations, that give more precise results in comparison to simulation in 2D design environment, which is described in the IEC 60099-4 standard. The fact that the electric field is dependent not only upon the height and the distance of the measurement position, but also upon the selected axis, creates the need of the 3D representation of the arrester, in order to obtain better estimations of the electric field distribution around the arrester. For first time, simulation results are compared to experimental measurements, in order to confirm the appropriateness of the developed models. Additionally, the measurement results are accompanied with their total expanded uncertainty, making more accurate the comparison procedure.

The two designed models can be useful for the computation of the voltage distribution along the varistor, which cannot be measured, since it is impossible to reach the varistor inside the arrester. Via the used software the voltage distribution can be calculated easily and precisely, once the desirable geometry is accurately designed. The models can also be used to try changes of geometry or materials in order to achieve lower values of the electric field and more uniform voltage distribution of the arrester.

## References

- [1] Hinrichsen V. Metal-oxide surge arresters fundamentals[R]. 1st ed. [S.l.]: Siemens, 2001.
- [2] ABB Buyer's Guide. High voltage surge arresters[R]. [S.l.]: ABB, 2004.

- [3] James R E, Su Q. Condition assessment of high voltage insulation in power system equipment[M]. 1st ed. London, UK: The Institution of Engineering and Technology, 2008: 83-84.
- [4] Vahidi B, Nasab R S, Moghani J Sh, *et al*. Three dimensional analyses of electric field and voltage distribution on ZnO surge arrester with broken sheds[C]//2005 IEEE/PES Transmission and Distribution Conference & Exhibition. Dalian, China: IEEE, 2005: 15-18.
- [5] Meshkatoddini M R. Study of the electric field intensity in bushing integrated ZnO surge arresters by means of finite element analysis[C]//COMSOL Users Conference 2006. Boston, USA: [s.n.], 2006: 22-24.
- [6] Lundquist J, Stenstrom L, Schei A, *et al*. New method of the resistive leakage currents of metal-oxide surge arresters in service[J]. IEEE Transactions on Power Delivery, 1990, 5(4): 1811-1822.
- [7] Heinrich C, Hinrichsen V. Diagnostics and monitoring of metal-oxide surge arresters in high-voltage networks-comparison of existing and newly developed procedures[J]. IEEE Transactions on Power Delivery, 2001, 16(1): 138-143.
- [8] IEC 60099-4: E.2.1 Surge arresters: part 4: metal-oxide surge arresters without gaps for AC systems[S], 2006.
- [9] Vahidi B, Nasab R S, Moghani J S. Analysis of electric field and voltage distributions on ZnO surge arrester for polluted condition[C]//Proceedings of the XIVth International Symposium on High Voltage Engineering. Beijing, China: Tsinghua University, 2005: 25-29.
- [10] Tighilt F, Bayadi A. Computed voltage distribution in ZnO arrester under pollution by finite element method[C]//4<sup>th</sup> International Conference on Computer Integrated Manufacturing CIP'2007. Setif, Algeria: [s.n.], 2007: 3-4.
- [11] Karthik R. A novel analysis of voltage distribution in zinc oxide arrester using finite element method[J]. International Journal of Recent Trends in Engineering, 2009, 1(4): 1-3.
- [12] Han S J, Zou J, Gu S Q, *et al*. Calculation of the potential distribution of high voltage metal oxide arrester by using an improved semi-analytic finite element method[J]. IEEE Transactions on Magnetics, 2005, 41(5): 1392-1395.
- [13] Christodoulou C A, Spanias S A, Gonos I F, *et al*. Electric field measurements around a metal oxide surge arrester[C]//Proceedings of the 2010 International Conference on High-Voltage Engineering and Application (ICHVE 2010). New Orleans, USA: [s.n.], 2010: 278-281.
- [14] IEC 60060-1 High voltage test technique, part 1: general definitions and test requirements[S], 1989.
- [15] Narda. System for the electromagnetic fields measurement (PMM 8053A) [R]. [S.I.]: Narda, 2004.
- [16] Narda. Field analyzer for LF fields, selective and broadband (Narda EFA-200/300) [R]. [S.I.]: Narda, 2003.
- [17] IEC 60-2 High voltage test-techniques, part 2: Measuring systems[S], 1996.
- [18] Vector Fields Limited. OPERA-2d reference manual[R]. Oxford Shire, England: Vector Fields Limited, 2009.
- [19] Vector Fields Limited. OPERA-3d reference manual[R]. Oxford Shire, England: Vector Fields Limited, 2009.



**Christos A. Christodoulou** was born in 1983 in Lamia, Greece, where he ended the primary and the secondary education. He studied in the School of Electrical and Computer Engineering of the National Technical University of Athens (2001 - 2006) and he carried out his PHD thesis in the High Voltage Laboratory (2006-2010). He speaks English, German and Italian. He participates to tests and measurements, and he is also a laboratory assistant at the High Voltage Laboratory of

the National Technical University of Athens. Additionally, he designs electrical (low and medium voltage) and mechanical installations. His scientific interests concern on high voltages, lightning protection and electromagnetic compatibility. He is author of 10 papers in Conference Proceedings and 7 papers in International Scientific Journals.

E-mail: Christ\_fth@yahoo.gr



**Chrysovalantis Spanias** was born on 21st of December in 1985 at Limassol, Cyprus. He studied Electrical Engineering and Computer Engineering in National Technological University of Athens on 2005 until 2010. He was interested on high voltages. now is working as a consultant and contractor electrical engineer in Cyprus.

E-mail: vtechaos@yahoo.gr



**Vassiliki T. Kontargyri** was born in 1978 in Athens, Greece, where she ended the primary and the secondary education. She received the diploma in Electrical and Computer Engineering from the National Technical University of Athens in 2002 and the Ph.D. degree from the same university in 2007. She worked in the Public Power Corporation S.A. (2000). Since 2002 she teaches laboratory lessons at the Department of Energy Technology in the Faculty of Technological Applications of the

Technological Education Institute of Athens. She was also a teaching assistant at the Hellenic Naval Academy (2003-2008). She is working at the High Voltage Laboratory of NTUA. Her research interests concern grounding systems, insulators, high voltages, measurements and neural networks. She is the author of more than 40 papers in scientific journals and conferences proceedings.

E-mail: vkont@power.ece.ntua.gr



**Ioannis F. Gonos** was born on May 8, 1970 in Artemisio, Arcadia, Greece. He received his diploma in Electrical Engineering and his Ph.D. from the National Technical University of Athens in 1993 and 2002 respectively. He is a lecturer with the School of Electrical and Computer Engineering, National Technical University of Athens (Since May 2013). He was a researcher at the High Voltage Laboratory of the National Technical University of Athens (January 2002-

April 2013). He was a laboratory assistant at the High Voltage Laboratory and Photometry Laboratory of the National Technical University of Athens (1996-2013), at the Hellenic Naval Academy (1996-2001) and at the Department of Energy Technology in the Faculty of Technological Applications of the Technological Education Institute of Athens (1996-2001). His research interests concern grounding systems, insulators, high voltages, measurements, electromagnetic compatibility, and genetic algorithms. He is the author of more than 130 papers in scientific journals and conferences proceedings. He is member of Technical Chamber of Greece, IEEE and CIGRE.

E-mail: igonos@cs.ntua.gr



**Ioannis A. Stathopoulos** was born in Volos, Greece in 1951. He studied in the Faculty of Electrical and Mechanical Engineering of the National Technical University of Athens (1969-1974). He carried out his doctor thesis at the Technical University of Munich (1974-1978). He became teaching assistant at the Technical University of Munich (1974-1978), production engineer in the company "Vianox-Franke" (1979-1980), teaching assistant at the National Technical

University of Athens (1979-1983) and thereafter lecturer (1983-1987), assistant professor (1987-1991), associate professor (1991-1995) and professor (since 1995) in the High Voltage Laboratory of the NTUA. He is the author of 8 books and more than 170 papers in scientific journals and conferences proceedings. He is lead assessor of the Hellenic Accreditation Council.

E-mail: stathop@power.ece.ntua.gr

Received date 2012-11-08

Editor YAN Meng